



Empirical Characterization of Ground Motions for Induced Seismicity in Alberta

Mark Novakovic¹, Gail M. Atkinson², Karen Assatourians³

¹ Research Scientist, Nanometrics, Kanata, ON, Canada.

² Professor, Department of Earth Science, Western University - London, ON, Canada.

³ Research Scientist, Department of Earth Science, Western University - London, ON, Canada.

ABSTRACT

Over the last decade instances of induced seismic activity resulting from waste water injection and hydraulic fracture treatments have increased significantly both in rate and maximum magnitude of observed events. Evaluation of the induced-seismicity hazard requires development of appropriate ground-motion prediction equations (GMPEs). A region-specific GMPE is developed using a selected and compiled database of over 880 ground motion observations in Alberta, including 37 events of moment magnitude 3.0 to 4.3, recorded over the hypocentral distance range from 5 to 575 km, and primarily associated with hydraulic fracture operations. A generalized inversion is used to solve for regional source, attenuation parameters, and station site responses, within the context of an equivalent point-source model, following the method of Atkinson et al. [1]. The resolved parameters include the regional geometric spreading and anelastic attenuation functions, source parameters for each event, a regional near-surface high-frequency attenuation term (κ_0), and site response terms for each station relative to a reference site condition (B/C boundary). The parameters fully specify a regionally-calibrated GMPE that can be used to describe median amplitudes from induced earthquakes in Alberta. The GMPE can be implemented to estimate magnitude, stress and median ground motions in near-real time, which is useful for ground-motion-based alerting systems and traffic light protocols. The derived GMPE has further applications for the evaluation of hazards from induced seismicity.

Overall, the ground motions for B/C site conditions for induced events in Alberta are of similar amplitude at low frequencies to those predicted by the GMPEs of Yenier & Atkinson [2], Atkinson [3], for events of M 3 to 4.5. Alberta motions present lower amplitudes at high frequencies than those observed in Oklahoma, but are fairly consistent with the model of Yenier and Atkinson [2] for very shallow events in CENA.

Keywords: Induced seismicity, empirical ground motion prediction equation

INTRODUCTION

Induced seismic activity attributed to hydraulic fracturing and waste water injection operations has become more prevalent over the last decade [4-8]. A pressing issue is the potential hazard to infrastructure as a result of ground motions from induced earthquakes [9]. Regions with relatively low historic seismicity rates, that are located within the stable craton, and are distant from zones of tectonically active structures, will be associated with relatively low hazard. The introduction of induced seismicity to these regions may increase the probabilities of exceeding damaging ground-motions, and can drastically alter the hazard regime. Thus, it is important to characterize ground motion from these events, such that their contribution to hazard may be quantified. Recent monitoring programs launched by Universities (Western University, University of Alberta, and University of Calgary, in partnership with Nanometrics, Inc.), and by the Alberta Geological Survey, as well as the Geological Survey of Canada (with GeoScience British Columbia) have resulted in densification of the seismographic network, and improved the availability of ground-motion datasets for induced events in the Western Canada Sedimentary Basin (WCSB, in western Alberta and eastern B.C.). Nevertheless, the ground-motion data in the WCSB is sparse in comparison to those available in other regions, such as California and Oklahoma. Therefore, we can extend our understanding of motions in the WCSB by comparing them to those in more data-rich regions. Understanding of ground motions is fundamental to hazard assessment.

A region-specific GMPE for Alberta (median horizontal component) is developed using a generalized inversion to solve for regional source, attenuation and site responses following the method of Atkinson et al. [1] within the context of an equivalent-point-source model. The resolved parameters include the regional geometric spreading, anelastic attenuation,

source parameters for each event (magnitude scaling and stress parameter for a Brune point-source model), and site response terms for each station, referenced relative to the NEHRP (Natural Earthquakes Hazards Reduction Program) B/C site class boundary (time-averaged shear-wave velocity in the upper 30 m of 760 m/s). These parameters fully specify a regionally calibrated GMPE that can be used to describe median horizontal-component amplitudes across the region for hazard and ShakeMap applications, and to aid in the development of traffic light protocols and other risk-mitigation tools. Alberta ground motions are placed into context by comparing the resulting GMPE with one derived for Oklahoma induced seismicity by Novakovic et al. [10] (denoted as NAA18); NAA18 was calibrated using a larger ground-motion dataset than any previous GMPE study for induced events in North America. Further comparisons of GMPEs derived from waste-water injection and hydraulic-fracture induced seismic events with GMPEs determined from natural events in CENA and California are made.

METHODOLOGY

Database

More than 1000 earthquakes of $M > 2.5$ were reported in Alberta from August 2013 to July 2018. We select 884 from 37 events at 75 seismograph stations with $M > 3$. Records are queried for RAVEN, CN, MB networks from IRIS, waveforms for the TransAlta network (TD) are provided by Nanometrics, and 6 months of continuous waveforms from the Canadian Rockies and Alberta Network (CRANE) were provided by the University of Alberta. Waveforms were processed and compiled to produce a geometric mean of the horizontal component ground motion database, consisting of 5%-damped pseudo spectral acceleration (PSA), peak ground acceleration (PGA) and peak ground velocity (PGV). PGA and PGV are computed from the absolute maximum amplitude of the corresponding time series. PSAs are calculated from the corrected time series using a modified version of the ICORRECT algorithm [11], which utilizes the Nigam and Jennings [12] algorithm, sampled at 30 log-spaced frequencies from 0.2 Hz to 50.0 Hz. Moment magnitude (M) is estimated for each event from the spectral amplitude of the low-frequency end of the spectrum using the method as shown in NAA18 [10]. The magnitude-distance distribution, as well as a map of event and station locations of the compiled database is shown in Figure 1.

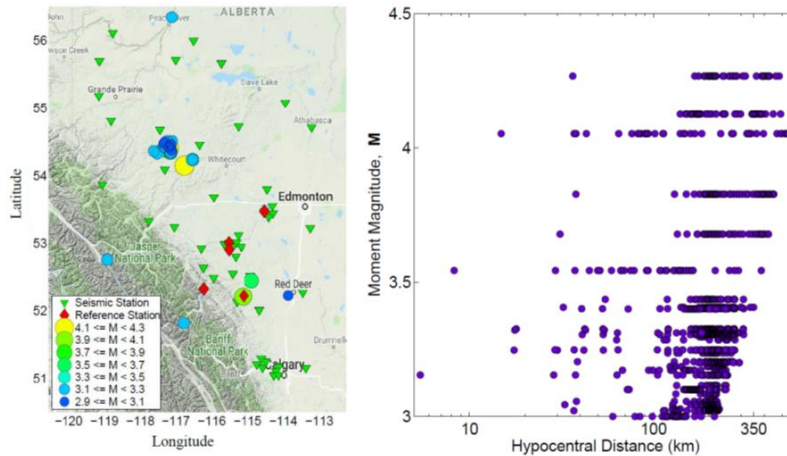


Figure 1. (Left) map of event and station locations used in study. (Right) magnitude-distance distribution of database.

Ground Motion Prediction Equation

Following the methodology of Atkinson et al. [1] we begin with a generic GMPE

$$\ln(\mathbf{Y}_T) = \mathbf{F}_z + \mathbf{F}_M + \mathbf{E}_i + \mathbf{F}_s + \mathbf{F}_r \quad (2)$$

Where: $\ln(\mathbf{Y})$ is the ground motion observation, such as the PGA, PGV or pseudo spectral acceleration (PSA) at a select frequency. \mathbf{F}_z , \mathbf{F}_M , \mathbf{E}_i , \mathbf{F}_s , and \mathbf{F}_r are the geometric spreading term, magnitude scaling term, event term (contains the stress parameter function $\mathbf{F}_{\Delta\sigma}$, a referenced high frequency attenuation function \mathbf{F}_κ and empirical calibration factor \mathbf{C}), site effects and anelastic attenuation parameter respectively (all in \ln units). We assume the magnitude scaling term \mathbf{F}_M as developed in Yenier and Atkinson [13]. \mathbf{F}_z is a modified tri-linear version of the Yenier and Atkinson [13] geometric spreading function of

hypocentral distance (\mathbf{R}), transition zone attenuation coefficient b_2 , transition distances R_T , a reference distance term that accounts for near-distance saturation, and a correction factor F_{Fourier} which accounts for the difference between modelling amplitudes in the Fourier domain versus the spectral domain[13], as follows:

$$\mathbf{F}_Z = \begin{cases} -1.3 * \ln(\mathbf{R}) + F_{\text{Fourier}} & \text{for } \mathbf{R} \leq R_{T1} \\ -1.3 * \ln(R_{T1}) + b_2 * \ln\left(\frac{\mathbf{R}}{R_{T1}}\right) + F_{\text{Fourier}} & \text{for } R_{T1} < \mathbf{R} \leq R_{T2} \\ -1.3 * \ln(R_{T1}) + b_2 * \ln\left(\frac{R_{T2}}{R_{T1}}\right) - 0.5 * \ln\left(\frac{\mathbf{R}}{R_{T2}}\right) + F_{\text{Fourier}} & \text{for } R_{T2} < \mathbf{R} \end{cases} \quad (3)$$

$$F_{\text{Fourier}} = (b_3 + b_4 \mathbf{M}) \ln\left(\frac{\mathbf{R}}{R_{\text{ref}}}\right) \quad (4)$$

We adopt a frequency-independent geometric spreading model allowing frequency-dependent effects to be carried by the anelastic attenuation coefficient; this is consistent with nearly all previous stochastic models of ground motion (e.g. [1, 13, 14, 15, 10]). To define the shape of the trilinear form, we first assume that the anelastic attenuation and stress parameter models derived in NAA18 are valid in Alberta and remove the magnitude scaling and anelastic attenuation functions. Residual ground motion trends are plotted against R_{hypo} at each frequency. Model parameters are chosen that broadly match the shape across all frequencies, suggesting that a trilinear geometric spreading function with transition distances R_{T1} and R_{T2} of 90 km and 160 km respectively and attenuation slopes b_1 , b_2 , b_3 of -1.3, 1.3, and -0.5 respectively is appropriate for the region. Yenier [16] developed a local magnitude relation for the Western Canadian Sedimentary Basin (WCSB) that introduced a trilinear distance correction model to correct for the decay in Wood-Anderson amplitudes, which features a steep transition zone that agrees well with that found in this study.

A trade-off exists in ground-motion modeling between stress parameter and the near- surface high-frequency attenuation slope, kappa (κ_0) [17]. Observations of high frequency attenuation in Alberta facilitated the need to incorporate a kappa correction term. Yenier and Atkinson [13] used a fixed kappa and site condition to constrain this trade-off. Hassani and Atkinson [18] extended their model to allow variable site conditions and kappa combinations, by introducing a kappa term (F_κ) and site response term (F_s) in the response spectral domain. The kappa term is defined by the following polynomial [18]:

$$F_{\kappa_0} = \sum_{i=0}^4 e_{\kappa_0,i} [\log_{10}(\kappa_0)]^i \quad (5)$$

where $e_{\kappa_0,i}$ are magnitude-dependent coefficients. Because the kappa term is 0 for the reference value of $\kappa_0 = 0.001$ s, it is required that

$$e_{\kappa_0,0} = 3e_{\kappa_0,1} - 9e_{\kappa_0,2} + 27e_{\kappa_0,3} - 81e_{\kappa_0,4}. \quad (6)$$

The magnitude-dependent coefficients for each of the $i = 1-4$ of the F_{κ_0} functional form can then be expressed as

$$e_{\kappa_0,i} = \sum_{j=0}^3 P_{i,j} [\log_{10}(\mathbf{M})]^j \quad (7)$$

and stress-parameter-dependent coefficients of $e_{\kappa_0,i}$, $P_{i,j}$ can be written as

$$P_{i,j} = \sum_{n=0}^2 d_{i,j,n} [\log_{10}(\Delta\sigma)]^n \quad (8)$$

in which $d_{i,j,n}$ are the coefficients of $P_{i,j}$ for each oscillator frequency, $i = 1-4$, $j = 0-3$, and $n = 0-2$. The Yenier and Atkinson [2] model implicitly applies to $\kappa_0 = 0.025$ s, so we chose to reference the kappa term (F_κ) from Eq (2) to this value as:

$$F_\kappa = F_{\kappa_{AB}} - F_{\kappa_{0.025}} \quad (9)$$

where $F_{\kappa_{AB}}$ is the F_{κ_o} function evaluated for the kappa term determined for Alberta, and $F_{\kappa_{0.025}}$ is the F_{κ_o} function evaluated for the reference kappa of 0.025s. The kappa function is evaluated for the frequencies which coefficients are provided in Hassani and Atkinson [18], then interpolated to the frequencies used in this study for both the regional kappa term determined for Alberta and the reference kappa term.

Station terms F_s are expressed relative to a reference NEHRP site condition. Seismograph stations thought to be located on sites with time-averaged shear-wave velocities in the top 30 m (V_{s30}) of ~ 760 m/s are chosen as reference sites, with respect to which all other site responses will be determined. Farrugia et al. [19] suggest that generally the site condition in Alberta is C-D, based on a combination of H/V ratio analysis and results from site-specific studies. H/V ratios are used as an initial guide to selection of sites likely to be suitable reference sites as shown in the electronic supplement of Farrugia et al. [19]. We select five reference sites, which are post-hole installations thought to be coupled near bedrock and have well-behaved horizontal to vertical component ratios that are broadly similar to each other and consistent with those expected for near B/C sites based on other studies [20]. Moreover, we restrict our reference station selection to the stiffest sites available, as determined by Farrugia et al. [19] using surface ambient noise vibration. The inversion constraint applied is that the average site amplification over these selected reference stations at each frequency is zero. Any differences between the actual amplification of the five sites (on average) and that assumed for B/C sites in the underlying generic GMPE of Yenier and Atkinson [2], will be cast into the calibration constant (C) by the inversion.

RESULTS

Application to Alberta Ground-Motions

Eq. (2) is rearranged and through a generalized inversion [21] the stress parameter, near-surface attenuation adjustment function, site effect term, anelastic attenuation and calibration factor are solved for frequency by frequency for each region. To facilitate inversion, the assumed trilinear geometric spreading function and Yenier and Atkinson [2] magnitude scaling term are removed from ground motion observations:

$$\ln(Y_{ij}) - F_{M,i} - F_{Z,i,j} = E_i + F_{S,j} + \gamma R_{\text{hypo } ij} \quad (10)$$

The frequency dependent anelastic attenuation parameter, γ , is shown in Figure 2. At low frequencies, the attenuation is stronger than typically observed in CENA, weaker than that in California, and comparable to that of Oklahoma as determined

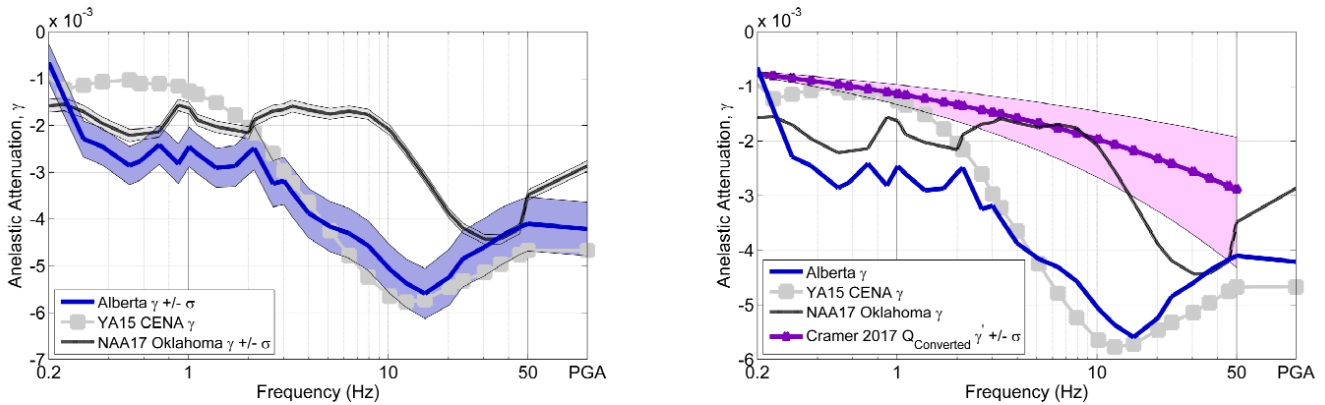


Figure 2. Comparison of anelastic attenuation in Alberta, Oklahoma and Central and Eastern North America.

in NAA18 [10] as well as Q-converted anelastic attenuation determined in Cramer [22]. At intermediate to high frequency, the Alberta γ term follows closely to that of CENA, and is stronger than that for Oklahoma.

As expected, the peak amplifications for many sites are significant; in some cases exceeding a factor of five at specific frequencies. Figure 3 shows the reference stations as well as a sample of typical site response functions from non-reference stations. The average response is consistent with our understanding that the sites range from NEHRP class C to E (e.g. [19]).

The event term (E_i) determined by the inversion implicitly includes the event-specific stress adjustment factor for each event, average near-surface site effects for the reference sites, and the regional calibration factor. NAA18 [10] based the

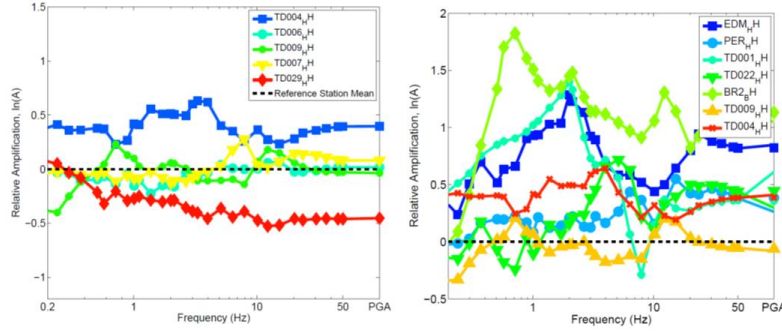


Figure 3. (Left) site amplification functions for reference stations. (Right) sample site amplification terms.

stress parameter on the event's average high-frequency spectral level, as represented by PSA at 10 Hz, relative to that expected based on the seismic moment, accounting for any offset in amplitude level at the moment-end of the spectrum. For event terms in Alberta, we observed that high-frequency level tends to be best expressed in the frequency range from 6.00 to 8.00 Hz. We used the event term as evaluated at 6.30 Hz to represent the high-frequency level for each event. This is similar to the shape-based approach of Yenier and Atkinson [2] but focuses on the high-frequency spectral level relative to the low-frequency level, instead of focusing on the corner frequency. For ease of application in implementing this approach, the generic GMPE of Yenier and Atkinson [2] was evaluated at 20 km for multiple combinations of magnitude and stress parameter, then is used to define the relationship between 6.30 Hz PSA and stress parameter:

$$\log_{10}(\Delta\sigma) = 2.024 + 1.52(\log_{10}(PSA_{6.3\text{Hz},\text{event}}) - (\log_{10}(PSA_{6.3\text{Hz},100\text{bar}}) + \Delta LF)) * \max(1, 1.3 \left(\frac{3.5}{M}\right)) \quad (11)$$

where $PSA_{6.30\text{ Hz},\text{event}}$ is the average 6.3 Hz PSA value for the event, adjusting for site and path effects to the reference distance of 20 km, and $PSA_{6.30\text{ Hz},100\text{bar}}$ is the corresponding 6.30 Hz PSA that is predicted for a Brune stress parameter of 100-bar at 20 km. This parameterization makes it easy to back-calculate the stress parameter from the 6.30 Hz value of the event spectrum at 20 km. The basic idea is that we are using the high-frequency spectral level to infer the corner frequency, instead of using the corner frequency to infer the high frequency level (as was done in Yenier and Atkinson [2]). This approach was found to be more stable by NAA18 [10], leading to a lower standard deviation of determined stress parameters.

The stress parameter increases with magnitude for small events and the values fall within the range that would be expected (eg. [2, 10]). A wide range of stress parameter values, typically from 10 to 200 bars, are observed for events of $M > 3$. It has been suggested that stress increases with focal depth, and that this is the primary reason why induced events typically have a lower stress parameter than do natural tectonic earthquakes (e.g. [2, 23, 10]). Catalog depths for the events (Table A2) fall predominantly in the range from 1 to 10 km, however the errors in depth calculations are often larger than the measurement itself, precluding any meaningful interpretation of depth effects within the source terms. In Figure 4, stress parameters are plotted as a function of magnitude against models for CENA and Oklahoma and compared to values determined for suspected induced events in other studies (eg. [24, 25, 26, 10]). Stress parameters determined for hydraulic fracture induced events in Alberta lie within the range of stress drop values for waste water injection induced events in Oklahoma, as determined through other techniques (Fourier spectral fitting and empirical Greens functions). Goertz-Allmann et al. [27] computed stress drops for 1000 events induced by geothermal water injection in a deep borehole in Basel, Switzerland. Stress drops typically range from 2 to 200 bar, and on average fall within 20 to 50 bar between $M_{0.5}$ -3.0 respectively. These values are consistent with what Wu et al. [26] observed for injection induced events in Oklahoma for events $M < 3.0$. On average the stress parameter from Alberta events follow the YA15 CENA models events having a depth of about 6 km [2]. For this depth the stress dependence on magnitude is given by YA15 [2] as:

$$\ln(\Delta\sigma) = 4.544 + \min[0, 0.229(M - 5.0)]. \quad (12)$$

We determine the best near-surface attenuation parameter (κ_0) for Alberta through an iterative grid-search process. For each event we evaluate the magnitude scaling term; remove the reference κ term by subtracting the F_{κ} function evaluated at 0.025

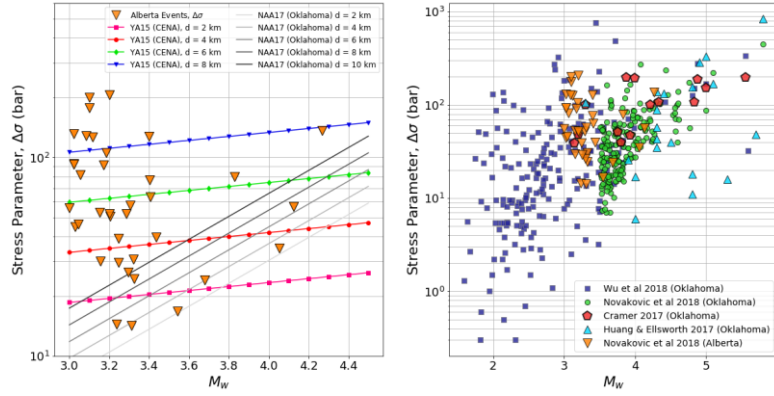


Figure 4. (Left) stress parameters determined by inversion for each event as a function of M (triangles). Solid lines show the stress parameter model for Oklahoma evaluated over a range of depths. Lines with symbols depict YA15 stress parameter models for CENA over a range of depths. (Right) Composition of stress parameter computations in this study with suspected induced events in Oklahoma from other studies.

s ($F_{\kappa_{0.025}}$); then evaluate the stress parameter function for a suite of logarithmically-spaced stress parameter values; and evaluate the κ function for linearly-spaced kappa terms, using:

$$E_{pred,i,j} = F_M + F_{\Delta\sigma,i} + F_{\kappa_j} - F_{\kappa_{0.025s}} \quad (13)$$

By comparing the spectrum predicted by the event term $E_{pred,i,j}$ for each stress-kappa pair against the value determined for the event using the approach outlined above, for frequencies from 0.90 Hz to 24.0 Hz, we determine the best fit stress-kappa pair for each event, as well as all pairs that fit above the 97.5th, 95th and 90th percentiles. This allows us to observe the acceptable range of stress-kappa pairs for each event and evaluate the trade-off between these two parameters. These two terms have a proportional relationship such that if one parameter is increased, the other follows. We next fix the stress parameter values for each event to match the model given by Eq. (12) and grid search for the best mean kappa term. For the stress parameter values given in Eq. (12), the corresponding κ_0 that best matches the observed event term to the model generally lies between 0.05 s and 0.07 s. Based on these analyses, we select a mean value of 0.06 s as the average regional kappa term for soil sites in Alberta.

The regional calibration factor (C) is determined as the residual mismatch between the observations and the model (after considering the modeled stress parameter for each event, the site term for each station, and the regional kappa, geometric spreading and anelastic attenuation functions). As discussed in Yenier and Atkinson [13], the calibration factor reflects the average differences between the observations and the simulations, including any systematic factors that are not accurate or not included in the modeling approach. Examples of such factors include any residual regional site amplification effects relative to the assumed amplification model for B/C that was included in the Yenier and Atkinson [2] formulation, and any surface wave or other contributions to the motion that were not included in the Brune source model. Removing the resolved parameters from the inversion from the ground motion observations, Eq. (2) becomes

$$\ln(Y_{ij}) - F_{M,i} - F_{Z,i,j} - \gamma_{AB}R_{ij} - F_{\Delta\sigma} - F_{S_j} - F_{\kappa_0} = C_{AB} + \eta_i + \varepsilon_{ij} \quad (14)$$

where C_{AB} is the regional calibration factor for Alberta, η_i is the between-event error, and ε_{ij} is the within-event error. Following Abrahamson and Youngs [28], we use a mixed effects regression of residuals to solve Eq. (14). An iterative regression is performed to maximize the likelihood of the model and estimate the regional calibration factor (C_{AB}). The residual error of the observations with respect to the model is separated into its between-event and within event components (η_i and ε_{ij}). At frequencies < 0.30 Hz we observe a positive residual of up to 0.5 ln units at 0.20 Hz. This is explained by microseismic contributions and inherent limitations of stochastic methods at low frequencies, which do not allow surface wave phases or coherent pulses to be properly modeled. We suggest using a constant value of 0 at $f < 0.2$ Hz to prevent mapping the micro seismic peak at low frequencies to larger magnitudes. The calibration factor dips steadily from 0 to -0.5

In units between 0.2 Hz to 2.23 Hz where it remains relatively constant to 50.0 Hz. A suggested calibration factor model for Alberta is given by:

$$C_{AB} = \begin{cases} 0 & \text{for } f < 0.3 \text{ Hz} \\ -0.69 \log_{10}(f) - 0.36 & \text{for } 0.2 \text{ Hz} \leq f < 1.59 \text{ Hz} \\ -0.50 & \text{for } f \geq 1.59 \text{ Hz} \\ -0.39 & \text{for PGV} \\ -0.36 & \text{for PGA} \end{cases} \quad (15)$$

The shape of the calibration function at intermediate frequencies might reflect deviations from the regional site response model assumed for the reference B/C condition. The generic GMPE form upon which this study is based has embedded within it a prescribed average crustal amplification function for B/C conditions, which was derived from an assumed model [29].

The final GMPE for Alberta includes the assumed magnitude scaling and geometric spreading functions, the derived model for the anelastic attenuation terms, stress parameter, site amplification terms, and the empirical calibration factor, and is described as:

$$\ln(Y_{ij}) = F_M + F_{\Delta\sigma,AB} + F_Z + F_\gamma + F_S + F_{\kappa_0} + C_{AB} \quad (20)$$

In Figure 5a we plot the within-event residuals ($\varepsilon = \ln(\text{observed}) - \ln(\text{predicted})$) for the horizontal-component (geometric mean) PSA at 1.01 Hz as well as the final GMPE (for PSA at 1.0 Hz), overlaying site-corrected observations. There are no significant trends in the residuals in magnitude or distance, for hypocentral distances greater than 50 km; at closer distances, there is a tendency towards slightly positive residuals at some frequencies, and slightly negative at others.

In Figure 5b, we compare the GMPE for induced events in Alberta, at 1.00 Hz, to: the Oklahoma GMPE of NAA18 [10] evaluated at the mean focal depth of induced events in Oklahoma of 5 km; the CENA GMPE of Yenier and Atkinson [2] for earthquakes at depths of 2 and 5 km, for events of **M3** and **M5**, respectively; and the GMPE of Atkinson [3], which was derived from moderate events with an average depth of 9 km in California (NGA-West2 database), but postulated to apply for induced events, is also shown. For low-to-intermediate frequencies the tri-linear geometric spreading function generally traces the level of Yenier and Atkinson (denoted as YA15) [2] and Atkinson [3] where the GMPE predicts slightly lower amplitudes near the first transition and slightly higher near the second transition zone. At higher frequencies the GMPE derived for Alberta is generally low for near to intermediate distances (<150 km) and matches the level at far distances when compared to YA15 and Atkinson [3].

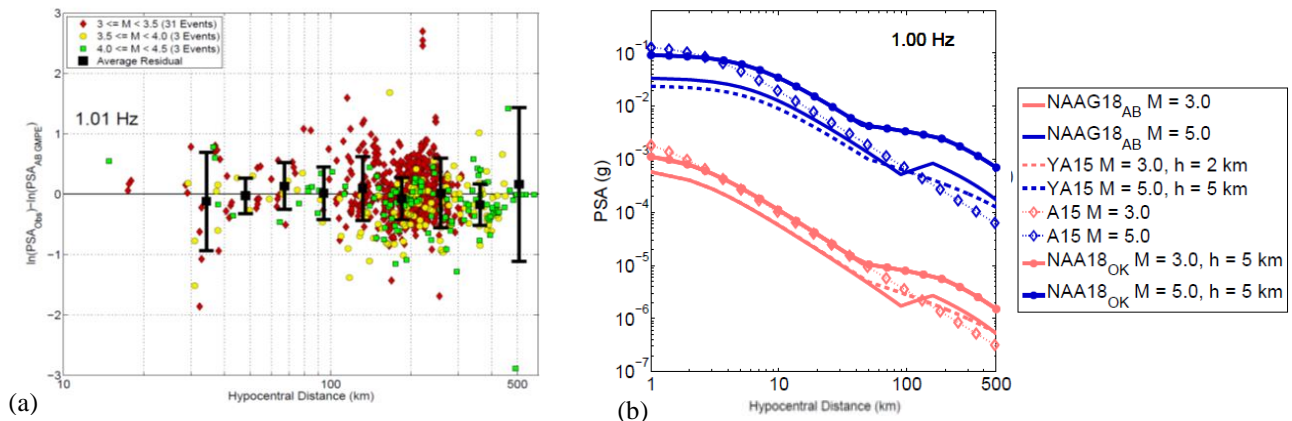


Figure 5. (a) within event residuals (predicted ground motions subtracted from observations) at 1.01 Hz. (b) final GMPE evaluated for **M3** and **M5** (solid lines) at 1.00 Hz in comparison with the NAA18 [10] GMPE evaluated at 5 km depth for Oklahoma (circles), the GMPE of Atkinson (2015) [3] for shallow events in California (diamonds), and the Yenier and Atkinson (2015) [2] GMPE for CENA evaluated for **M3** and **M5** at 2 and 5 km depths respectively (dashed lines).

Alberta ground motion amplitudes are generally lower than those observed in Oklahoma [10], especially at high frequencies (> 10 Hz). Differences of amplitude in the Alberta and Oklahoma GMPEs reflect the differences in stress parameter models. Alberta events appear to follow the CENA model of YA15 [2] evaluated at 6 km depth, whereas in Oklahoma the derived model (involving both depth and magnitude) features higher stress parameters [10]. This could reflect generally greater depths for induced events in Oklahoma, or some other differences attributable to source processes. Differences in average regional crustal amplification may also contribute to the difference in observations as these will map into the source terms.

CONCLUSIONS

A regionally-adjusted GMPE for induced events in Alberta is developed that describes the geometric mean of horizontal component PSA, PGV, and PGA ground motions for a reference condition of B/C. The generic GMPE framework of Yenier and Atkinson [2] is used to ensure stable scaling of motions over all magnitudes and distances. We calibrate the generic GMPE by determining site amplification models, anelastic attenuation function, regional stress parameter model, adapted regional near surface high frequency attenuation term [18], and calibration factor from > 880 ground-motion observations from Alberta events of $M \geq 3$ at hypocentral distances from 20 to 575 km. The derived GMPE is useful for ShakeMap applications, hazard assessments and may also be useful for ground-motion-based alerting systems and traffic light protocols.

ACKNOWLEDGMENTS

We would like to thank NSERC & TransAlta for funding this project. We also thank Nanometrics for providing the locations of detected events in Alberta.

REFERENCES

- [1] Atkinson, G. M., Hassani, B., Singh, A., Yenier, E., Assatourians, K. (2015). Estimation of Moment Magnitude and Stress Parameter from ShakeMap Ground-Motion Parameters. *Bull. Seismol. Soc. Am.* DOI: 10.1785/0120150119.
- [2] Yenier, E., and Atkinson, G. M. (2015b). Regionally-Adjustable Generic Ground-Motion Prediction Equation based on Equivalent Point-Source Simulations: Application to Central and Eastern North America. *Bull. Seismol. Soc. Am.* 105(4), 1989-2009.
- [3] Atkinson, G. M. (2015). Ground-motion prediction equation for small to-moderate events at short hypocentral distances, with application to induced seismicity hazards, *Bull. Seismol. Soc. Am.* 105, 2A, doi: 10.1785/0120140142
- [4] Ellsworth, W. (2013). Injection-Induced Earthquakes, *Science* 341, 1225942.
- [5] Keranen, K., Weingarten, M., Abers, G., Bekins, B., and Ge, S. (2014). Sharp Increase in Central Oklahoma Seismicity Since 2008 Induced by Massive Wastewater Injection, *Science* 345, 448-451.
- [6] Schultz, R., Stern, V., Novakovic, M., Atkinson, G. M., Gu, Y. (2015). Hydraulic Fracturing and the Crooked Lake Sequences: Insights Gleaned from Regional Seismic Networks. *Geophysical Research Letters*. Doi:10.1002/2015GL063455.
- [7] Atkinson, G., Eaton, D., Ghofrani, H., Walker, D., Cheadle, B., Schultz, R., Shcherbakov, R., Tiampo, K., Gu, J., Harrington, R., Liu, Y., van der Baan, M., and Kao, H. (2016). Hydraulic fracturing and seismicity in the Western Canada Sedimentary Basin, *Seismological Research Letters* 87, no. 3, doi: 10.1785/0220150263.
- [8] Petersen, et al. (2016). USGS Open-File Report 2016-1035, <https://pubs.er.usgs.gov/publication/70182572> (Last accessed November 2016).
- [9] Atkinson, G. M. (2017). Strategies to prevent damage to critical infrastructure from induced seismicity. *FACETS*, *Science Application Forum*, doi: 10.1139/facets-2017-0013
- [10] Novakovic M., Atkinson G. M., Assatourians K. (2018). Empirically Calibrated Ground-Motion Prediction Equation for Oklahoma. *Bull. Seismol. Soc. Am.* DOI: 10.1785/0120170331
- [11] Assatourians, K., and Atkinson, G. M. (2010). Database of processed time series and response spectra for Canada: An example application to study of the 2005 MN 5.4 Riviere du Loup, Quebec earthquake, *Seismol. Res. Lett.* 81(6), 1013–1031.
- [12] Nigam, N. C. and Jennings, P. C. (1969). Calculation of Response Spectra from Strong-Motion Earthquake Records, *Bull. Seismol. Soc. Am.* 59(2), 909-922.
- [13] Yenier, E., and Atkinson, G. M. (2015a). An Equivalent Point-Source Model for Stochastic Simulation of Earthquake Ground Motions in California. *Bull. Seismol. Soc. Am.* 105(3), 1435-1455.
- [14] Boore, D. M. (2003). Simulation of ground motion using the stochastic method, *Pure and Applied Geophysics* **160**, 635-675.
- [15] Atkinson, G. M. and Boore D. M. (2006). Earthquake ground-motion prediction equations for eastern North America, *Bull. Seism. Soc. Am.* 85, 17-30.
- [16] Yenier, E. (2017). A Local Magnitude Relation for Earthquakes in the Western Canadian Sedimentary Basin, *Bull. Seismol. Soc. Am.* DOI: 10.1785/0120160275
- [17] Anderson, J. G., and Hough S. E. (1984). A model for the shape of the Fourier amplitude spectrum of acceleration at high frequencies, *Bull. Seismol. Soc. Am.* 74, 1969 – 1993.
- [18] Hassani, B., and Atkinson G. M. (2018). Adjustable Generic Ground-Motion Prediction Equation Based on Equivalent Point-Source Simulations: Accounting for Kappa Effects. *Bull. Seismol. Soc. Am.* 108(2), 913-928.
- [19] Farrugia, J. J., Atkinson, G. M., Molnar, S. (2017). Validation of 1D Earthquake Site Characterization Methods with Observed Earthquake Site Amplification in Alberta, Canada. *Bull. Seismol. Soc. Am.* 108 (1): 291-308.
- [20] Ghofrani H. and Atkinson G. M. (2014). Site Condition Evaluation Using Horizontal-to-Vertical Response Spectral Ratios of Earthquakes in the NGA-West2 and Japanese Databases. *Soil Dynamics and Earthquake Engineering*, 67, 30-43.
- [21] Andrews, J. (1986). Objective determination of source parameters and similarity of earthquakes of different size, *Earthquake Source Mechanics*, American Geophysical Union, *Geophysical Monograph*, 37, 259-267.
- [22] Cramer, C. (2017). Gulf Coast Regional Q and Boundaries from USArray Data. *Bull. Seismol. Soc. Am.* 108(1), 437-449
- [23] Assatourians, K., and Atkinson, G. M. (2017). Are Ground-Motion Models Derived from Natural Events Applicable to the Estimation of Expected Motions for Induced Earthquakes? *Seism. Res. Lett.* DOI: 10.1785/0220160153.
- [24] Cramer, C. (2017). Brune Stress Parameter Estimates for the 2016 M_w Pawnee and Other Oklahoma Earthquakes. *Seismological Research Letters*, 88(4):1005-1016.
- [25] Huang, Y., Ellsworth, W. L., and Beroza, G. C. (2017). Stress drops of induced and tectonic earthquakes in the central United States are indistinguishable. *Science Advances* 3(8), e1700772.
- [26] Wu, Q., Chapman, M., Chen, X. (2018). Stress-Drop Variations of Induced Earthquakes in Oklahoma. *Bull. Seismol. Soc. Am.* 108 (3A), 1107-1123.
- [27] Goertz-Allmann, B. P., Goertz, A., Wiemer, S. (2011). Stress drop variations of induced earthquakes at the Basel geothermal site. *Geophysical Research Letters*, 38, L09308, doi:10.1029/2011GL047498
- [28] Abrahamson, N. A., and R. R. Youngs (1992). A stable Algorithm for regression analysis using the random effects model, *Bull. Seismol. Soc. Am.* 82(1), 505–510.